Chemical Engineering Journal 492 (2024) 152263

Contents lists available at ScienceDirect

Chemical Engineering Journal

journal homepage: www.elsevier.com/locate/cej

Self-healing hydrogel reduces inflammation through ANT1/OPTN axis mediated mitophagy for spinal cord injury repair

Xiaohua Dong [a,b,c,1], Jing Zhao [a,1], Dongya Jiang [a], Ziyi Lu [a], Xingdan Liu [a], Kaijia Tan [a], Kelvin W.K. Yeung [f], Xuanyong Liu [d,e,*], Liping Ouyang [a,b,c,*]

[a] Laboratory of Key Technology and Materials in Minimally Invasive Spine Surgery, Tongren Hospital, Shanghai Jiao Tong University School of Medicine, Shanghai 200336, China
[b] Department of Anesthesiology, Tongren Hospital, Shanghai Jiao Tong University School of Medicine, Shanghai, China
[c] Hongqiao International Institute of Medicine, Tongren Hospital, Shanghai Jiao Tong University School of Medicine, Shanghai, China
[d] State Key Laboratory of High Performance Ceramics and Superfine Microstructure, Shanghai Institute of Ceramics, Chinese Academy of Sciences, Shanghai, China
[e] College of Biological Science and Medical Engineering, Donghua University, Shanghai, China
[f] Shenzhen Key Laboratory for Innovative Technology in Orthopaedic Trauma, Guangdong Engineering Technology Research Center for Orthopaedic Trauma Repair, Department of Orthopaedics and Traumatology, The University of Hong Kong Shenzhen Hospital, Shenzhen, China

ARTICLE INFO

Keywords:
Self-healing hydrogel
Spinal Cord Injury
Inflammation
Mitophagy

ABSTRACT

Spinal cord injury is hard to repair due to the aggregated injury to neighbor cells caused by neuro-inflammation, which always results in severe outcomes. In this work, Tc peptide, which served as the antagonist of CXCR4 and the agonist of CXCR7, was loaded in a self-healing hydrogel. The hydrogel containing Tc was found to possess superior spinal cord injury repair abilities, including motor neuron regeneration, axon bridging repair and motor functions recovery, due to the inflammation inhibition. The mechanism analysis by RNA-sequencing and *in vitro* experiments found that the elevated ANT1 accelerates OPTN recruitment, which subsequently recognized by LC3 to form phagophore around dysfunctional mitochondria, resulting in a regressive NLRP3 expression. However, this regression was abolished after inhibiting OPTN. Beneficial from the mitophagy process, ROS was reduced and type 1 microglia activation was diminished. This positive feedback loop accelerated spinal cord injury repair. In summary, the hydrogel containing Tc could promote spinal cord injury repair through reducing neuro-inflammation *via* enhanced ANT1/OPTN axis mediated mitophagy, which may provide a new peptide containing hydrogel for repairing spinal cord injury.

1. Introduction

Spinal cord injury (SCI) caused by trauma is worldwide concerned issue due to the severe outcomes. The life quality of patients would be badly affected by the loss of action capacity [1]. Neuro-inflammation is one of the culprits of amplified damage of SCI due to the followed actions, including oxidation/nitridation stress, calcium overload, mitochondrial damage and energy disorders, which cause extensive injury in neurons [2]. Microglia is the resident macrophage in central nervous system that plays essential role in cellular debris clearance and neuro-restorative processes [3]. Infection induced pathogen associated molecular pattern (PAMP) and trauma induced damage associated molecular pattern (DAMP) activate microglia to an amoeboid activated phenotype. The classical activated microglia secrets pro-inflammatory cytokines, chemokines, and reactive oxygen species (ROS) to active immune response. Although these elevation of activation could accelerate pathogen and cellular debris clearance, the excessive and extensive activation may result in inhibition of axonal remodeling and neurogenesis through releasing pro-inflammation cytokines, such as tumor necrosis factor-α (TNF-α), inducible nitric-oxide synthase (iNOS), interleukin-1β (IL-1β), interleukin-6 (IL-6), ROS and so on [3,4].

Strategies applied to promote SCI through regulating microglia induced inflammation have been widely researched in the recent decades, including NO generator triggered by near infrared light [5], bone

* Corresponding authors at: State Key Laboratory of High Performance Ceramics and Superfine Microstructure, Shanghai Institute of Ceramics, Chinese Academy of Sciences, Shanghai, China (X. Liu). Laboratory of Key Technology and Materials in Minimally Invasive Spine Surgery, Tongren Hospital, Shanghai Jiao Tong University School of Medicine, Shanghai 200336, China (L. Ouyang).
E-mail addresses: xyliu@mail.sic.ac.cn (X. Liu), lpouyang@shsmu.edu.cn (L. Ouyang).
[1] These authors contributed equally to this work.

https://doi.org/10.1016/j.cej.2024.152263
Received 25 January 2024; Received in revised form 28 April 2024; Accepted 13 May 2024
Available online 14 May 2024

marrow stem cell derived exosome loading hydrogel [6], and peptide incorporated silk fibroin nanofiber [7]. As the degradation product of protein, peptide exhibits many advantages, such as low allergy, high pharmacodynamics, and low cost [8]. Many peptides have been proved to be beneficial for SCI regeneration. VD11 is the peptide derived from the amphibian spinal cord, which could promote axonal regeneration through activation of the AMPK and AKT signaling pathways [9]. ISP and PAP4 peptides play important roles in regeneration of spinal cord injury and recovery of motor function after peripheral nerve injury [10]. Additionally, the small-molecule, polypeptide neutrophil peptide (NP-1), promotes sciatic nerve regeneration after crush injury [11]. The peptide, Tc14012, which is the antagonist of CXCR4 and agonist of CXCR7 [12], has been known to promote the functions of endothelial progenitor cells for cardiac repair [13]. Recent references disclosed that CXCR4 inhibition also promotes neural functions [14,15]. Therefore, Tc14012 may be a new peptide that promotes the regeneration of spinal cord injury.

Hydrogel is one of the crosslinked polymer materials that possesses superior abilities to prolong the bio-active, prevent burst release, and maintain stable drug delivery concentration of bio-molecule. Several

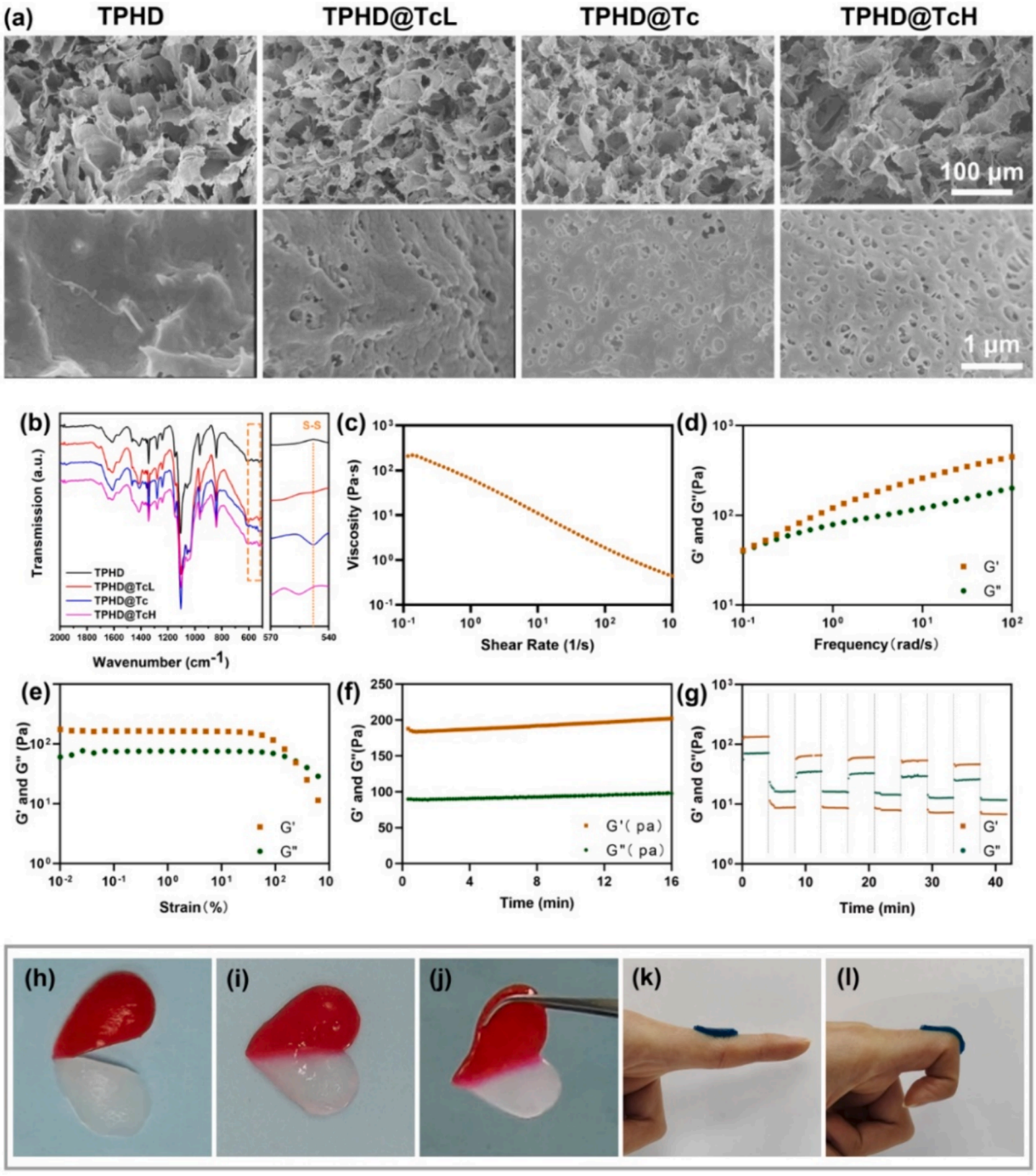

Fig. 1. Morphologies and surface properties of the samples. (a) Surface morphologies of the samples. (b) FTIR spectra of the samples. (c) Shear-thinning property of the hydrogel. (d) Frequency sweep test of the hydrogel at 1 % strain. (e) Oscillatory strain amplitude sweeps measurement of the hydrogel with the strain ranging from 0.01 % to 1000 %. (f) The change of storage modulus (G′) and loss modulus (G″) under 16 min test. (g) Self-healing property of the hydrogel with alternate strain between 1 % and 500 % at 25℃. (h-j) Self-Healing property of the hydrogel after cut. (k-l) Adhesion of the hydrogel.

hydrogels are prepared for nerve platform, including chitosan [16,17], hyaluronic acid (HA) [18], collagen [19], and silk fibroin based hydrogels [20]. Various bio-molecules have been proved to possess well delivery and bio-active after loading into hydrogels, such as vascular endothelial growth factor (VEGF) [21,22], nerve growth factor-2 (NGF) [23] and neurotrophin-3 (NT-3) [16,17,24]. Except for protein, hydrogels are also used for cell incorporation, which provide well support and fine environment for cell survive. For example, a myoglobin laden peptide hydrogel for cell grafts could sustainably maintain oxygen delivery, and thus improve cell survival, integration and differentiation [25].

Consequently, in this work, a triple composites hydrogel (TPHD) containing polyvinyl alcohol (PVA), polyethylene glycol (PEG) and hyaluronic acid (HA) were fabricated for loading Tc14012, which was beneficial for maintaining peptide bio-active and decreasing biotoxicity. Then, the surface morphology, rheological properties and self-healing ability were detected. A spinal cord injury model was constructed using transgenic zebra fish *(Tg* (*mnx1: GFP*), *Tg (lyzc: GFP)*, and *Tg (mpeg1: mCherry)*) to study the nerve repair and inflammation response *in vivo*. For further analyzing the mechanism, RNA-Seq and the related molecular biology experiment was applied to verify the pathways. Finally, the mitophagy and phenotype of microglia were observed.

2. Results

2.1. Materials characterizations

The hydrogels were lyophilized and the morphologies were observed. Fig. 1**a** showed that all the hydrogels had a three-dimensional porous structure. Moreover, no obvious drug particles were seen in the hydrogel of the drug-carrying group, indicating that Tc can form a homogeneous substance with the hydrogel. Compared with TPHD, the characteristic peak of S-S appeared in the TPHD@TcL and TPHD@Tc at about 547 cm^{-1}. While a little shift was observed in TPHD@TcH due to the more hydrogen bond than TPHD@TcL and TPHD@Tc. The above results indicated that Tc was successfully loaded into the gel system (Fig. 1**b**). The negative correlation between the viscosity and shear rate were shown in Fig. 1**c.** The results indicated that the hydrogel showed shear-thinning behavior, which was beneficial for injecting (Fig. 1**d**). As shown in Fig. 1**e**, the strain at the intersection points of storage modulus (G') and loss modulus (G") of the hydrogel was determined to be 239 % by the strain scanning mode. When the strain exceeded the critical point, G' of the hydrogels dropped sharply and began to be lower than G", indicating that the gel network was destroyed and transformed into a solution state. The results of the time-dependent modulus change showed that the G' value of the hydrogel was higher than G", no crossover traces occurred, indicating the formation of a stable hydrogel (Fig. 1**f**). In addition, the self-healing property of the hydrogel was studied by a high and low strain cyclic scanning mode. In the test, a recycled oscillatory strain between 500 % and 1 % strain was applied to break and recover the hydrogel structure. As shown in Fig. 1**g**, when 500 % strain was applied, the G' value of the hydrogel decreased to less than G", indicating the collapse of the hydrogel network. Once the strain decreased to 1 %, G' almost returns to its original value, implying the recovery of the network. The above results demonstrated that the broken structure of the hydrogel could be recovered quickly and kept in the hydrogel state for at least 5 cycles.

The self-healing ability of the hydrogel was evaluated by the macroscopic healing test. A heart-shaped hydrogel was cut into two parts, one of which was colored red with pigment for better observation. Then, the two parts were reconnected at room temperature. The hydrogel healed after 30 min without any cracks and could be lifted without separation (Fig. 1**h-j**). To test the adhesion of the hydrogel, the hydrogel was photographed adhered to the finger joints and with twisting. The results showed that the hydrogel did not rupture during the twisting process, indicating that the hydrogel has good adhesion and toughness (Fig. 1**k-l**). The *in vitro* and *in vivo* degradation have been studied and the results were shown in Fig. S1**.** It could be observed from the degradation curve that the weight of hydrogel gradually decreases with the increase of degradation time, and the degradation rate of hydrogel exceeds 70 % both *in vitro* and *in vivo* at the 21st day.

2.2. Biocompatibility of hydrogel

To investigate the *in vivo* bio-toxicity of the hydrogel (TPHD) and hydrogel containing Tc (TPHD@Tc), the zebrafish larvae were co-cultured with different concentrations of TPHD and TPHD@Tc and the morphologies were observed at 48hpf and 72hpf. Based on the results, there was not any obvious morphological deficits in larvae treated with TPHD 20x, TPHD 100x, TPHD 500x, TPHD@ 20x, TPHD@ 100x, and TPHD@ 500x, respectively (Fig. 2**a and b**). The survival number of zebrafish larvae showed that there was not any negative effect on survival rate and hatching rate of zebrafish co-incubating with TPHD and TPHD@Tc compared with control group at 48hpf (Fig. 2**c and d**). The survival number was similar to hatching number, indicating that almost all of suvival zebrafish larvae hatched. Moreover, compared with control group, the heart rate and hatching number of zebrafish larvae in all experimental groups did not change significantly at 72hpf (Fig. 2**e**). These results indicated that the application of TPHD@Tc is safe *in vivo*. However, the same concentration of Tc had an obvious negative influence in survival, hatching, and morphology (Figs. S2 and S3). The above results indicated TPHD@Tc could diminish the drug toxicity due to its drug delivery abilities.

2.3. Hydrogel containing Tc promoted spinal cord injury repair

2.3.1. Motor neuron regeneration and axonal bridging repair

To determine the effect of hydrogels on nerve recovery after spinal cord injury, zebrafish SCI model was established using transgenic fish larvae (*Tg (mnx1:* GFP*)*), in which GFP was specifically expressed in neuron cells. Compared with the normal group, the SCI group, TPHD group and TPHD@Tc group had severe spinal cord interruption and resulted in an obvious degradation of motor neurons at 6hpi in the injury site (Fig. 3**a**). To determine the role of TPHD@Tc in motor neuron repair, the length of motor neurons in damaged site of zebrafish was quantified and the results were shown in Fig. 3**b**. The lengths of motor neurons were dramatically decreased in SCI (6.1 ± 11.8), TPHD (5.3 ± 6.3) and TPHD@Tc (5.7 ± 10.4) group than that of the normal group (113.2 ± 37.5) at 6hpi. While, the motor neuron length was significantly increased in TPHD@TC group compared with that in SCI group and TPHD group at 24hpi (65.2 ± 47.2 vs 18.9 ± 15.1 and 31.1 ± 35.8). Strikingly, motor neurons regeneration in TPHD@TC group (117.7 ± 39.5) almost reached a normal condition (121.7 ± 42.1) at 48hpi (Fig. 3b). For further study the influence of temperature and pH in biological activity of Tc, Tc was treated in different temperature (30 °C and 50 °C) and pH (5, 7, and 8) before hydrogel preparation. After that, the neural repair experiments were conducted and the results were shown in Fig. S4. The results showed that motor neuron repair and axonal bridging approached near-complete recovery using a hydrogel containing Tc at 48 hpi. These results suggested that temperature and pH variations do not adversely affect the biological activity of Tc.

To further determine the role of TPHD@Tc in axonal regrowth and recovery in spinal cord injury, the axonal bridging formation was examined at 6hpi, 24hpi and 48hpi, respectively. At 6hpi, the axonal bridging area of SCI and TPHD@Tc were comparable. At 24hpi and 48hpi, axonal continuity was remarkably increased ($p < 0.01$) in TPHD@Tc group compared with that in SCI groups (Fig. 3**c and d**). However, the axonal continuity was not recovery at 6 and 24hpi in TPHD group and there was little fluorescence in TPHD at 48 h (Fig. S5). The above results demonstrate that TPHD@Tc could accelerate the motor neuron regeneration and axonal regrowth in SCI zebrafish larvae.

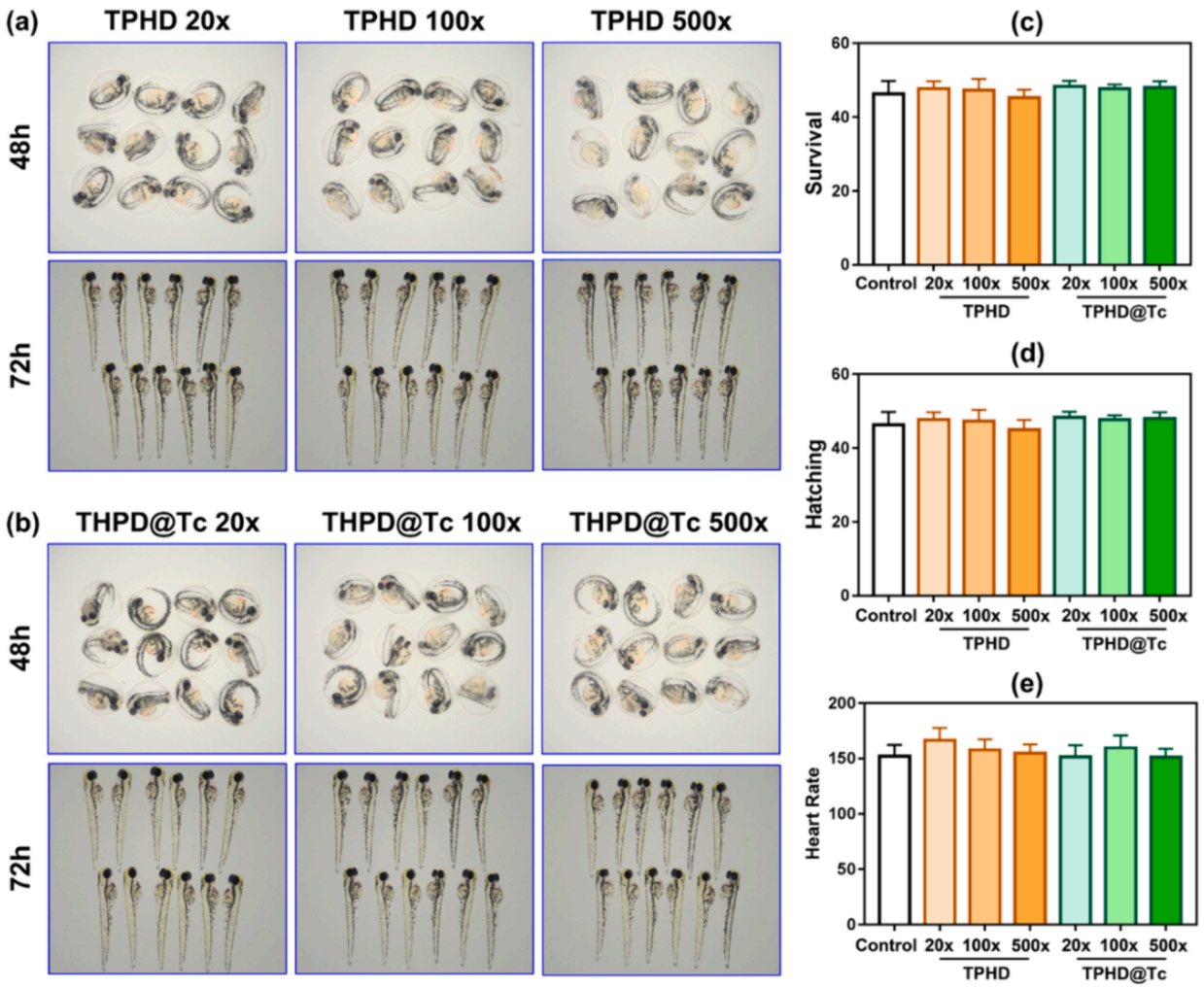

Fig. 2. Bio-toxicity of TPHD and TPHD@TC to zebrafish embryos. Morphologies of zebrafish treated with several concentrations of TPHD (a) and TPHD@Tc (b) for 48 h and 72 h. (c) Survival of zebrafish embryos treated with several concentrations of TPHD and TPHD@Tc for 48 h (n = 3). (d) Hatching of zebrafish larvae treated with several concentrations of TPHD and TPHD@Tc for 72 h (n = 3). (e) Heart rate of zebrafish larvae treated with several concentrations of TPHD and TPHD@Tc for 72 h (n = 15). Almost all of suvival zebrafish larvea hathed. Data were expressed by mean with SD. There is not any significance in c, d and e.

2.3.2. *Motor functions recovery*

To determine the functions recovery of locomotion, the swimming capacity analysis of the zebrafish larvae treated with TPHD and TPHD@Tc post SCI were performed and the results were shown in Fig. 4. The SCI model was constructed at 5 days, and the motor abilities were detected at 24hpi and 48hpi after SCI, respectively. The results showed that the swimming capability of SCI and TPHD groups were dramatically decreased compared with normal group, while the locomotive function of TPHD@Tc treated group was significantly improved at 24hpi and 48hpi (Fig. 4a and e). The velocity of TPHD@Tc group was dramatically increased compared with that in the SCI and TPHD groups at 24hpi and 48hpi, respectively (Fig. 4b and f). Consistent with velocity, the total movement distance of zebrafish increased significantly, and the cumulative immobility time decreased dramatically in the TPHD@Tc group compared with SCI and TPHD group at 24hpi and 48hpi (Fig. 4c-d and g-h). The above results suggested that TPHD@Tc plays a positive role in promoting the recovery of motor functions of zebrafish larvae after spinal cord injury.

The spinal cord injury model was conducted for further assessing the potential of TPHD@Tc in functional recovery of rats. Rats treated with TPHD@Tc post SCI achieved higher Basso, Beattie, and Bresnahan (BBB) scores at 5 days post SCI compared to TPHD, which exhibited that TPHD@Tc could significantly improve locomotor function (Fig. S6). HE staining was performed to examine the cavities of the injury site in TPHD and TPHD@Tc group at 21 days post-surgery. The results showed that disrupted tissue and large lesion volumes in the TPHD group. However, the group treated with TPHD@Tc displayed minimal cavitation, and the tissue regeneration exhibited an orderly arrangement (Fig. S7).

2.4. *Mechanism of hydrogel containing Tc in spinal cord injury repair*

2.4.1. *Hydrogel containing Tc inhibited macrophage and neutrophil activation*

Inflammatory response has been recognized to play a vital role in regeneration process of spinal cord injury [26]. In order to investigate the dynamic inflammation changes, *Tg(lyz: EGFP)* and *Tg(mpeg1: mCherry)* larvae were applied with SCI surgery, and the neutrophils and macrophages were observed by confocal microscopy. At 6hpi, Lyz + neutrophils were activated and accumulated in the injured site, the neutrophils fluorescence area was up to 189-fold in the SCI group compared with normal group. After treated with TPHD and TPHD@Tc in SCI zebrafish, neutrophils was reduced to 87.5 % and 51.9 %, compared with SCI group, respectively. And the neutrophils were dramatically decreased in TPHD@Tc group compared to TPHD group (n = 5, p = 0.0159) (Fig. 5**a and b**). Correspondingly, the neutrophils reduced to 35.9 % and 39.0 % in TPHD@Tc group compared to TPHD group at 24hpi and 48hpi post SCI, respectively (Fig. 5a and b). The effect of TPHD@Tc on macrophage modulation was observed too. The results

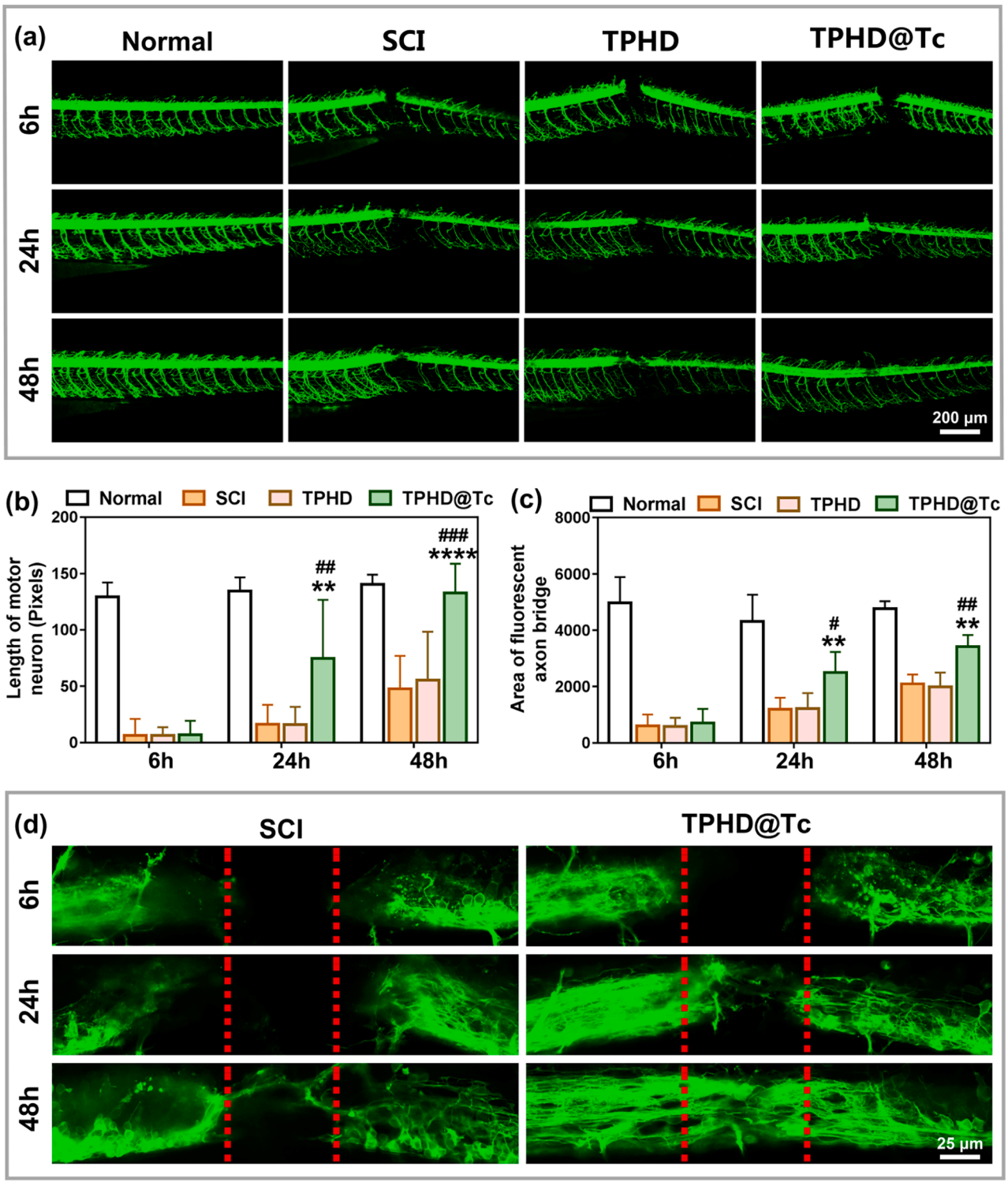

Fig. 3. Hydrogel containing Tc promoted motor neuron regeneration and axonal bridging repair after SCI. (a) Time course of motor neuron regeneration in Normal, SCI, TPHD and TPHD@Tc. (b) The lengths of motor neuron at 6hpi, 24hpi and 48hpi in Normal, SCI, TPHD and TPHD@Tc (n = 5). (c) Statistics of fluorescent area of axonal bridging in Normal, SCI, TPHD and TPHD@Tc at 6hpi, 24hpi and 48hpi (n = 5). (d) The axonal bridging in SCI and TPHD@Tc. The SCI injury site was labeled by red dotted line. Data were expressed by mean with SD. ** $p < 0.01$, **** $p < 0.0001$, compared with SCI in b and c. # $p < 0.05$, ## $p < 0.01$, compared with TPHD in b and c.

demonstrated that TPHD@Tc significantly ($p < 0.01$) diminished the population of macrophages in injured site compared to SCI at 24hpi (~29.1 %) and 48hpi (~21.3 %). In addition, TPHD@Tc dramatically decreased ($p < 0.01$) the population of macrophages in injured site compared to TPHD at 6hpf (~19.6 %), 24hpf (~52.4 %) and 48hpf (~37.9 %) (Fig. 5**c and d**). These results suggest that TPHD@Tc has a strong anti-inflammatory effect in zebrafish spinal cord injury.

The impact of TPHD@Tc in reactive oxygen species (ROS) accumulation was assessed and the results revealed that spinal cord injury (SCI) promoted an increase in ROS levels at 6-, 24-, and 48-hours hpi. Notably,

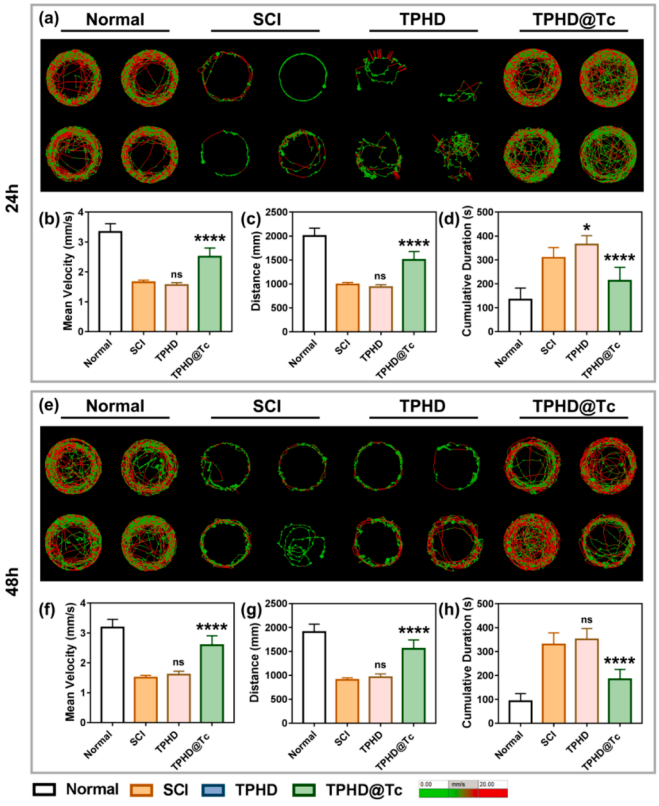

Fig. 4. Hydrogel containing Tc promoted motor functions recovery after SCI. (a) The movement trajectory of Normal, SCI, TPHD, and TPHD@Tc at 24hpi. The related quantification of the movement speed (b, n = 12), total movement distance (c, n = 12) and cumulative immobility time (d, n = 12). (e) The movement trajectory of Normal, SCI, TPHD, and TPHD@Tc at 48hpi. The related quantification of the movement speed (f, n = 12), total movement distance (g, n = 12) and cumulative immobility time (h, n = 12). Data were expressed by mean with SD. * $p < 0.05$, **** $p < 0.0001$, compared with SCI in b-d, f –h.

TPHD@Tc treatment resulted in a significant reduction in ROS production at 24 and 48 hpi, compared to SCI and TPHD-treated group (Figs. S8 and 9).

2.4.2. *ANT1 mediated NLRP3 downregulation involved in inflammation inhibition*

To further understand the potential molecular mechanism of TPHD@Tc in motor neuron repair and axon regeneration after SCI, we next performed RNA sequencing (RNA-seq) transcriptional profiling analysis of SCI regional (zebrafish trunk) in SCI and TPHD@Tc groups. RNA-seq analysis revealed that a total of 347 upregulated and 202 downregulated mRNA differentially expressed genes in TPHD@Tc group compared with SCI group ($p < 0.05$, $|\log_2 FC| > 0.58$). Notably, Gene Ontology (GO) enrichment analysis showed that the neuron projection regeneration was enriched from the upregulated genes and the inflammatory response was enriched from downregulated genes, which disclosed that the decreased neuron-inflammation was involved in spinal cord injury (Fig. 6**a and b**). Accumulation evidences suggest that dysfunction of autophagy would cause inflammation through excessive activation of NLR family pyrin domain containing 3 (NLRP3) inflammasome [27]. The intersection of autophagy-related genes based on the Autophagy Database and differentially expressed genes based on RNA-Seq revealed that there were three autophagy genes, adenine nucleotide transporter 1 (slc25a4, ANT1), eef2k and cdkn1a, might involve in the spinal cord injury recovery. In which, ANT1 and eef2k were upregulated and cdkn1a was downregulated in TPHD@Tc group (Fig. 6**c**). As the recent reference disclosed that ANT1 proudly affects mitophagy [28], which is related to regulate inflammation, the RT-qPCR and western blot were performed to assess the expression of ANT1 and NLRPL3 in BV-2 cells treated with hydrogels. The results showed that the mRNA and protein expression of ANT1 were dramatically elevated both in TPHD@Tc and TPHD@TcH groups compared with TPHD group (Fig. 6**d-e**). The fluorescent staining also showed that ANT1 was significantly increased in TPHD@Tc and TPHD@TcH group (Fig. 6**f and S10a**). Further, the inflammatory factor, NLRP3, was determined, and the results showed that it was significantly decreased both in TPHD@Tc and TPHD@TcH group compared with TPHD group (Fig. 6**g-i** and S10b). The above data indicated that TPHD@Tc promoted spinal cord injury repair via ANT1 mediated inflammation reduction. The variation of RNA level of ANT1 and NLRP3 is lighter than protein level in TPHD@TcH group (Fig. 6d-h). It is possible that TPHD@TcH influences not only the transcription levels of ANT1 and NLRP3 but also their post-translational regulation. Herewith, though the slighter variation of ANT1 and NLRP3 mRNA in TPHD@TcH, there is a larger change of protein.

2.4.3. *ANT1 enhanced OPTN recruitment promoted mitophagy mediated inflammation inhibition*

Reference disclosed that elevated ANT1 promoted optineurin (OPTN) recruitment, which subsequently enhanced mitophagy mediated inflammation inhibition. OPTN is one of the LC3 receptor which containing the Ub-binding domains (UBD) and LC3-interacting region (LIR), recognizing and binding LC3 on the autophagosome membrane through LIR. OPTN recognizes phosphorylated poly-Ub chains on mitochondrial proteins and initiates the formation of autophagosome via binding to LC3, thus promoting mitophagy [29]. Therefore, the co-located of translocase of outer mitochondrial membrane 20 (TOMM20, the marker of mitochondria) and OPTN (the protein recruited for mitophagy) were applied to disclose these pathways. Fig. 7**a-d** showed the co-location of TOMM20 and OPTN. As the results shown, there were OPTN cycles located around TOMM20 marked mitochondria, which indicated that OPTN was recruited to the mitochondria surface. While, the OPTN recruitment cycles could not be observed in TPHD and TPHD@TcL groups.

OPTN recruitment is beneficial for LC3 anchoring to form phagophore around dysfunctional mitochondria. The autophagy marker LC3B was detected by transfection BV2 cells with pCMV-LC3B-mCherry-GFP plasmid. When autophagy was activated, the plasmid expressed both mCherry and GFP. However, only mCherry was stably expressed when autophagosome combined with lysosome to form autophagolysosome. The results showed that the expression of mCherry, GFP and mCherry merged with GFP was dramatically increased in TPHD@Tc and TPHD@TcH group compared with TPHD group in BV2 cells treated with samples for 4 days (Fig. 7**e**). Autophagosome and autophagolysosome area calculated from the fluorescence staining showed that more autophagy can be observed in TPHD@Tc and TPHD@TcH group than TPHD and TPHD@TcL group. Quantitative results revealed that there were no significant differences between TPHD and TPHD@TcL group, while the fluorescence area of mCherry, GFP and mCherry mergered with GFP in TPHD@Tc and TPHD@TcH groups were remarkably higher than that in TPHD group (Fig. 7**f-h**). These results demonstrated that the TPHD@Tc could promote autophagy occurred in BV2 cells treated with TPHD@Tc. The above data disclosed that the elevated ANT1 promoted OPTN recruitment, which provided LC3 anchoring for phagophore formation around dysfunctional mitochondria, leading to a regressive inflammation (Fig. 7**l**).

To further determine the effect of ANT1/OPTN recruitment axis mediated mitophagy on inflammation, the OPTN expression was blocked by using Saikosaponin D (SSD, OPTN inhibitor). The results of qPCR and western blot showed that the inhibition effect of hydrogel containing Tc on NLRP3 was abolished. There were no significant differences in NLRP3 mRNA and protein expression among TPHD, TPHD@TcL, TPHD@Tc and TPHD@TcH groups after treated with SSD

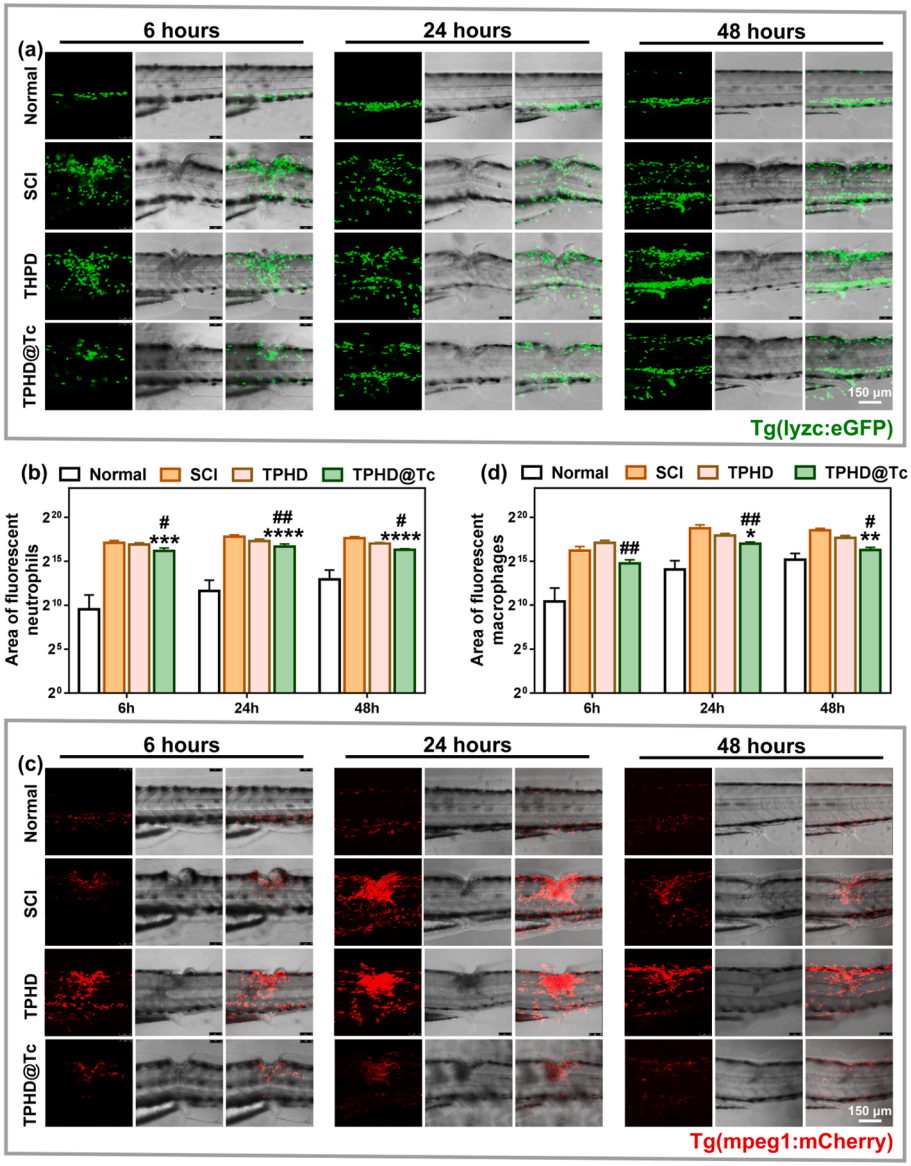

Fig. 5. Hydrogel containing Tc inhibited macrophage and neutrophil accumulation in the injured site. (a) The neutrophil population in Normal, SCI, TPHD and TPHD@Tc group at 6hpi, 24hpi, and 48hpi. (b) Statistics analysis of fluorescent area of neutrophil calculated from a (n = 5). (c) The macrophages response in normal, SCI, TPHD and TPHD@Tc group at 6hpi, 24hpi, and 48hpi, respectively. (d) Statistics analysis of fluorescent area of macrophages calculated from c (n = 5). Data were expressed by mean with SD. ** $p < 0.01$, *** $p < 0.001$, **** $p < 0.0001$, compared with SCI in b and c. # $p < 0.05$, ## $p < 0.01$, compared with TPHD in b and d.

(Fig. 7**i and j**). Similarly, the fluorescent staining showed that the expression of NLRP3 was consistent between SSD treated TPHD, TPHD@TcL, TPHD@Tc and TPHD@TcH groups (Fig. 7**k** and Fig. S11).

To further observe the effect of hydrogel containing Tc on microglia response, the proliferation, ROS activity and phenotype of BV2 were applied. Fig. 8**a** showed that the proliferation of BV2 treated with TPHD@TcL, TPHD@Tc and TPHD@TcH for 12 h, 24 h, and 96 h did not exhibit any obvious inhibitory effect compared with TPHD, which indicated hydrogel containing Tc has well biocompatibility to BV2 cells (Fig. 8a). LPS induced ROS production would amplify the damage post spinal cord injury. The immune-fluorescence staining was applied to further determine the ROS activity, and the results were shown in Fig. 8**b-d**. The TPHD@Tc and TPHD@TcH groups showed decreased ROS accumulation, about 34.9 % and 39.0 % decrease, compared to the TPHD-treated group at 1 day, respectively. While TPHD@TcL did not show any difference from TPHD at 1 day due to the lowest Tc content among these four groups containing Tc (Fig. 8b and d). ROS production of all groups decreased at 4 days. Similarly, the TPHD@Tc and TPHD@TcH group also showed a dramatic reduction ($p < 0.01$ and $p < 0.0001$) compared to TPHD group (Fig. 8c and d).

There is a positive feedback loop between ROS production and M1 polarization of microglia. Excessive oxidative stress activated microglia to M1 phenotype, which in turn produced ROS. To assess the role of hydrogel containing Tc in microglia polarization, immunofluorescence staining was performed. The results indicated that the expressions of Arg1 (M2 marker) in TPHD@Tc and TPHD@TcH group were significantly increased ($p < 0.01$ and $p < 0.001$), while the expression of iNOS (M1 marker) was remarkedly ($p < 0.001$ and $p < 0.0001$) decreased compared with TPHD and TPHD@Tc (Fig. 8**e-g**). Taken together, these results suggest that TPHD@Tc and TPHD@TcH plays an important role in ROS clearance and significantly promotes the polarization of LPS-stimulated microglia M1 to M2.

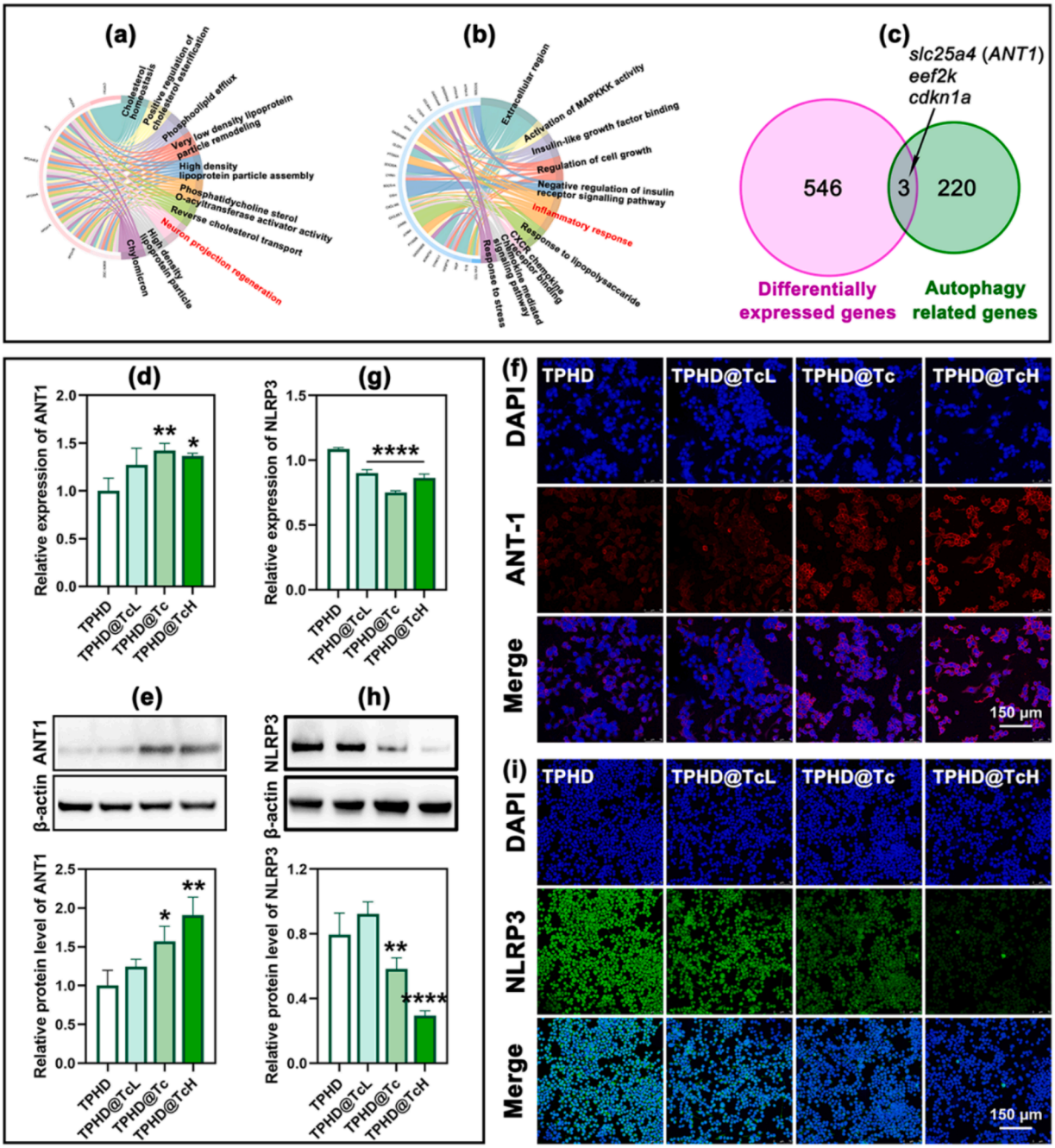

Fig. 6. RNA-seq analysis revealed that ANT1-mediated mitophagy involves in anti-inflammation effects. The top 10 upregulated enriched GO term (a) and the top 10 downregulated enriched GO term (b) of differentially expressed ($p < 0.05$, $|\log_2 FC > 0.58|$) mRNA in TPHD@Tc treated zebrafish compared with SCI group. (c) Veen analysis of the differentially expressed mRNA and autophagy-related genes. mRNA expression (d, n = 3), protein expression (e, n = 3) and Immunofluorescent staining (f) of ANT1 in BV2 cells treated with TPHD, TPHD@TcL, TPHD@Tc and TPHD@TcH for 4 days. mRNA (g, n = 3), protein expression (h, n = 3) and Immunofluorescent staining (i) of NLRP3 Data were expressed by mean with SD. * $p < 0.05$, ** $p < 0.01$, **** $p < 0.0001$, compared with TPHD in b and c.

3. Discussions

Spinal cord injury is hard to repair due to the complications post injury, including glial scar formation, neuron lost and axonal. The subsequent inflammation is one of the culprits, because the inflammatory cytokines participates many pathways to regulate neuron, astrocyte and microglia cells [30]. Microglia is the resident macrophage in the site of spinal cord, which polarizes to different phenotype to play essential functions in pro-inflammation and anti-inflammation. Cascade response of inflammation is the culprit for aggravated SCI injury due to the inflammatory cytokines and metabolites induced amplified damage of neighbor cells [31].

Many efforts have been done to lower the inflammation for SCI repair. The glutamate flooding out of neurons, axons and astrocyte in injured site produces ROS, which would cause neighbor cell death. For inhibiting this procedure, the biodegradable dextran based hydrogel was used to protect cells from the subsequent damage through alleviate ROS induced inflammation [6]. Another messenger, NO, is the molecule that can promote neural growth and regeneration. Zeolitic imidazolate framework–8 (ZIF-8) with CysNO was used to produce NO, which has been proved to suppress gliosis and inflammation [5]. In this work, we found that Tc, the antagonist of CXCR4, could obviously inhibit

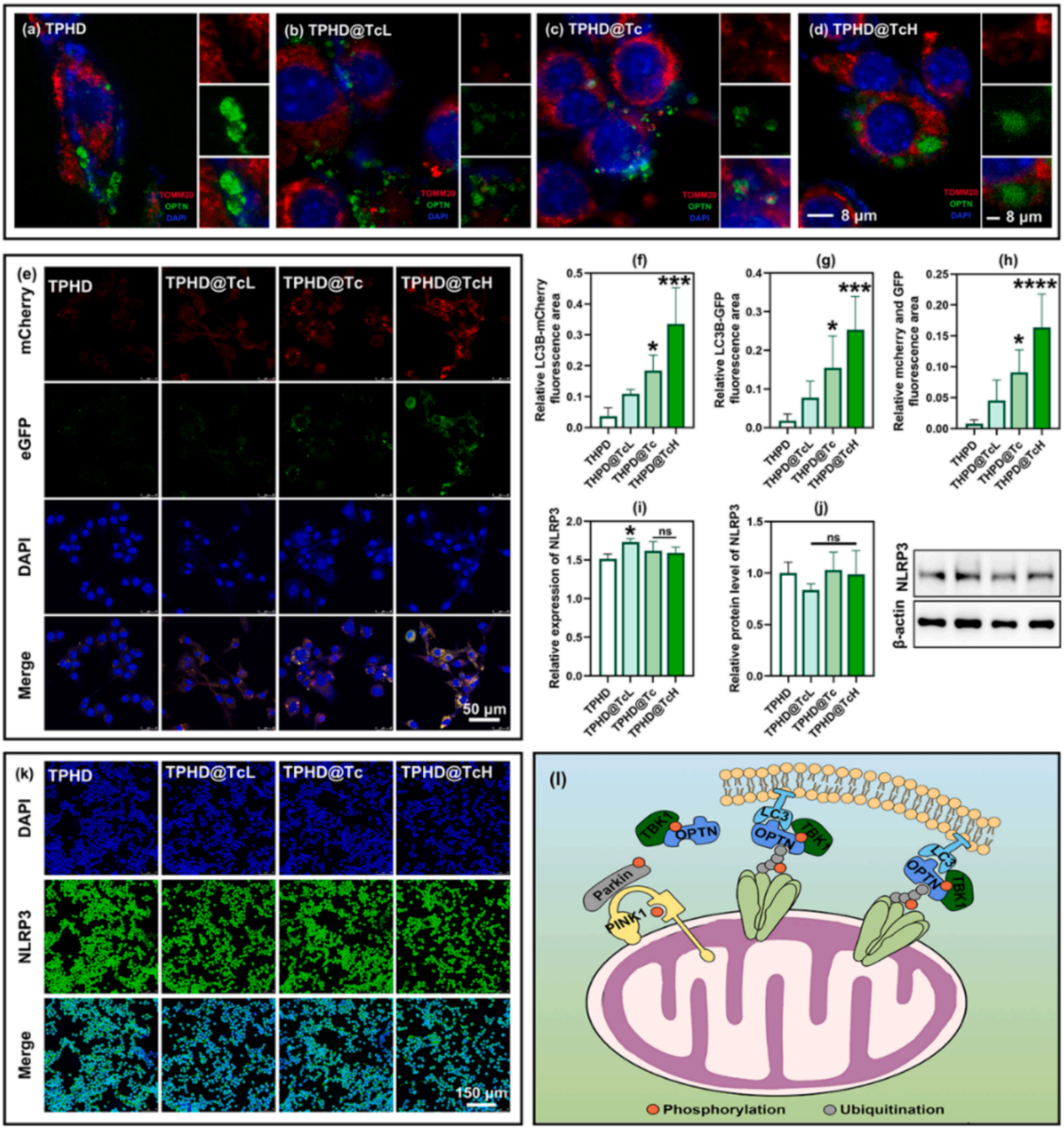

Fig. 7. ANT1 enhanced OPTN recruitment promotes mitophagy mediated inflammation inhibition. Immunofluorescence of TOMM20 (red) and OPTN (green) in BV2 cells treated with TPHD (a), TPHD@TcL (b), TPHD@Tc (c), TPHD@TcH (d) for 4 days. LC3B expression in BV2 cells treated with TPHD, TPHD@TcL, TPHD@Tc, TPHD@TcH for 4 days (e) and related quantitative m-cherry labeled area (f, n = 5), GFP labeled area (g, n = 5) and m-cherry and GFP co-labeled area (h, n = 5). NLRP3 mRNA expression (i, n = 3) and protein expression (j, n = 3) in BV2 cells treated with TPHD, TPHD@TcL, TPHD@Tc, TPHD@TcH for 4 days. Immunofluorescent staining of NLRP3 of BV2 cells treated with TPHD, TPHD@TcL, TPHD@Tc, TPHD@TcH for 4 days (k). (l) The schematic diagram of hydrogel containing Tc promoted mitophagy to decrease inflammation. The elevated ANT1 promoted OPTN recruitment, which provided LC3 anchoring for phagophore formation around dysfunctional mitochondria, leading to a regressive inflammation. Data were expressed by mean with SD. * $p < 0.05$, *** $p < 0.001$, **** $p < 0.0001$, compared with TPHD in f-j.

microglia (BV2) activating to type 1 and ROS production, which is beneficial for preventing the amplification of inflammation and secondary injury of cells. This found is consistent with the results of CXCR4 knockout. The CXCL12/CXCR4 signal axis mediated neuron regeneration is inhibited in the injured site, which leads to a failure of neuron repair [15]. Except for the CXCR4 related mechanism, we found that hydrogel containing Tc could suppress IL-1β and NOD-like receptor complex proteins (NLRPs) inflammasome expression.

NLRPs inflammasome triggered by trauma derived DAMP and infection derived PAMP is the platform that response to pro-inflammation environment and thus drive the process of pathogen and damaged cell clearance [32]. While, the caused excessive ROS would result in a delayed or failure tissue regeneration. Primary generated ROS induces mitochondrial dysfunction, which would further aggravate ROS and RNS (reactive nitrogen species) production [33]. Two independent pathways are involved in the regulation of dysfunctional mitochondrial,

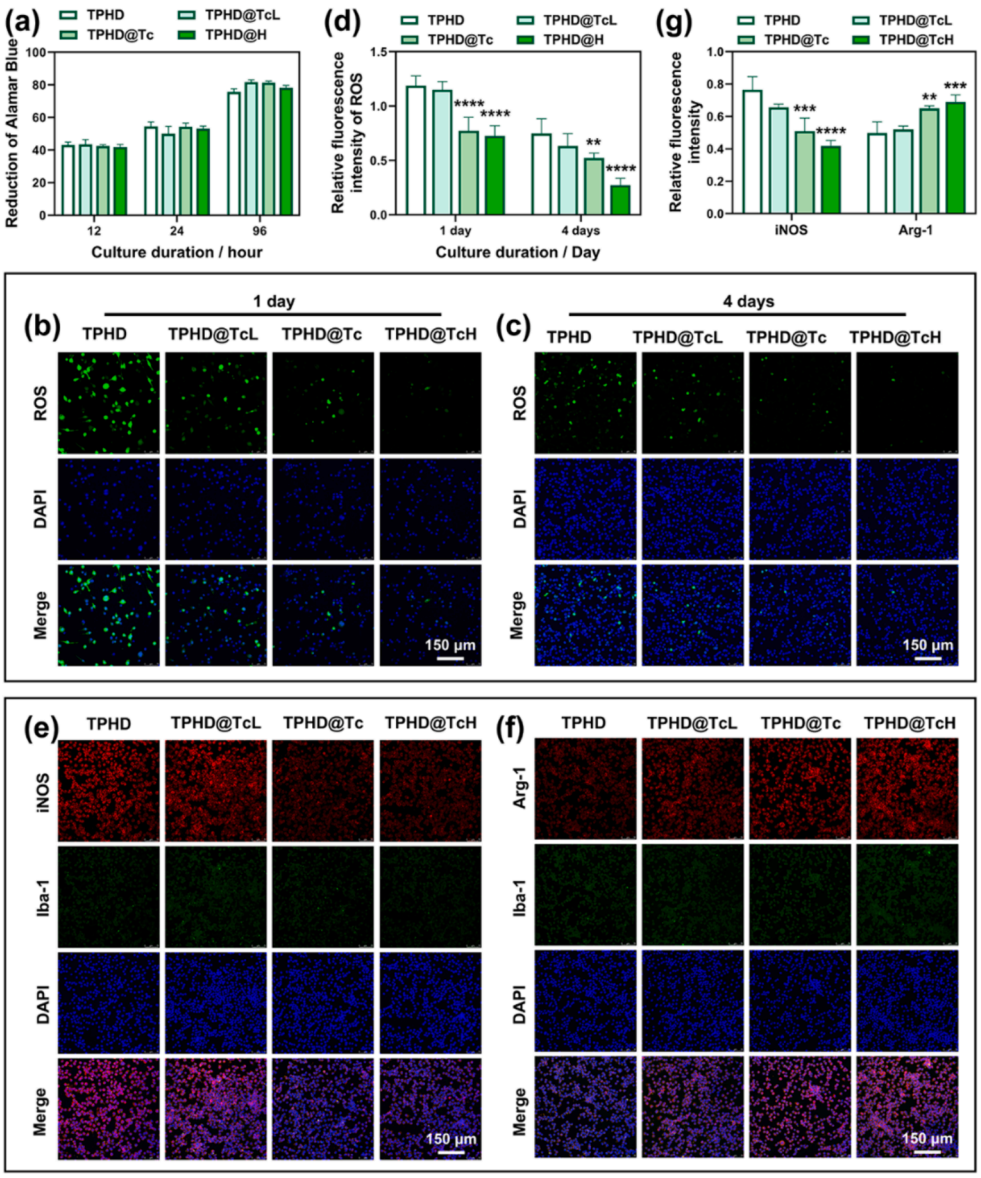

Fig. 8. Hydrogel containing Tc reduced ROS accumulation and M1 polarization. (a) Proliferation of BV2 cells treated with TPHD, TPHD@TcL, TPHD@Tc, TPHD@TcH for 12 h, 24 h and 96 h. Fluorescent staining of ROS of BV2 cells treated with TPHD, TPHD@TcL, TPHD@Tc, TPHD@TcH for 1 day (b) and 4 days (c) and relative statistical quantitative fluorescence intensity (d, n = 6). Co-location of Iba1 and iNOS (e), Iba1 and Arg-1 (f) of BV2 cells treated with TPHD, TPHD@TcL, TPHD@Tc, TPHD@TcH for 4 days. Relative statistical quantitative fluorescence intensity of iNOs and Arg-1 (g, n = 6). Data were expressed by mean with SD. ** $p <$ 0.01, *** $p < 0.001$, **** $p < 0.0001$, compared with TPHD in a, d and g.

which are NEMO related inflammation activation and OPTN related mitophagy [34]. Mitophagy is the process to maintain mitochondrial homeostasis through degrading damaged or dysfunctional mitochondria [35]. Mitophagy inhibition leads to ROS generating mitochondria accumulation and NLRPs inflammasome activation [32,36]. In this work, we found that TPHD hydrogel containing Tc could dramatically diminish NLRP3 and ROS production in LPS induced microglia cell, which may beneficial from the enhanced ANT1 mediated mitophagy. This diminishment effect of TPHD hydrogel containing Tc shows a positive dose dependent, while it is invalid strategy to enhance mitophagy and microglia through increasing Tc content.

ANT located on the inner membrane of mitochondria and was known to be the transport protein of ADP/ATP [37]. However, the recent research found that ANT participates in mitophagy and is independent of adenylate transport function[28]. In details, the activation of the classical PINK1/PARKIN autophagy signal depends on the opening and closing of the TIM23 membrane pore channel. ANT1 could combine with TIM44 and TIM23 to form a super complex, and thus keep membrane pore closed. PINK1 was prevented from degradation, and was phosphorylated for further Parkin combination. OPTN was then recruited for LC3 recognition to form phagophore. In this work, TPHD@Tc was verified to improve ANT1 expression, which enhances OPTN recruitment and autophagosome formation. The appropriate mitophagy could inhibit severe inflammation through removing damaged mitochondria. As a result, ROS was decreased, which further prevent macrophage polarizing to M1. Beneficial form the positive feedback loop, this effect could be amplified for inflammation inhibition.

4. Conclusions

Spinal cord injury is hard to repair due to the subsequent complications caused by microglia induced inflammation. In this work, the self-healing hydrogel containing peptide, Tc, was constructed for repairing

spinal cord injury. The zebrafish model shows that the hydrogel could promote neuron regeneration and axon bridging. The motor functions, including swimming velocity, distance and duration, of zebrafish treated with hydrogel containing Tc also recovered. The inflammation was inhibited post treating with hydrogel containing Tc, which was proved by the increased macrophage and neutrophil in the transgenic zebrafish treating with hydrogel containing Tc. Mechanism analysis found that the enhanced ANT1 mediated mitophagy reduced ROS and further diminished type 1 microglia activation. This positive feedback loop is beneficial for spinal cord injury repair.

5. Experimental section

5.1. Materials preparation and characterization

Preparation of the hydrogel: 1.5 g of polyvinyl alcohol (PVA) was dissolved in 15 mL sterilized water at 90 °C to obtain 100 mg/ml PVA solution. Subsequently, 150 mg of polyethylene glycol (PEG), 150 mg of hyaluronic acid (HA), and 15 mg of β-cyclodextrin (β-CD) were added to 6 ml of Tc14012 solution at different concentrations. After dissolving at room temperature, 3 ml of PVA solution was added to it and stirred rapidly for a few seconds to form hydrogel. The final concentration of Tc14012 in the hydrogel was adjusted to 0 mg/ml, 0.016 mg/mL, 0.032 mg/mL and 0.064 mg/mL respectively. The choose of the Tc content was based on the reference [38]. Finally, the hydrogels were subjected to repeated freeze-thawing at −20 °C for four times, each time for more than 12 h. The resultant hydrogels were recorded as TPHD, TPHD@TcL, TPHD@Tc and TPHD@TcH, respectively.

Materials characterizations: The microstructure of the hydrogels was observed using a scanning electron microscope (Scios 2, Thermo Scientific, USA). Before observation, the hydrogels were lyophilized and sprayed with gold. The chemical structures of the hydrogels were characterized by Fourier transform infrared spectroscopy (Thermo Fisher IS5).

Rheological properties of the hydrogel: The rheological behavior of the hydrogel was measured using a rheometer (MCR 102e, Anton Parr, AUT). Before test, the hydrogel was loaded on the parallel plate with a diameter of 25 mm. The strain amplitude sweep test was performed to analyze the value of the critical strain region of the hydrogel with a strain range of 0.1 to 1000 %. Frequency scanning test conditions were set as: constant strain 1 %, constant frequency 1 Hz, temperature 25 °C and frequency scanning range 0.1–100 rad/s. Then, the self-healing ability of the hydrogel was evaluated under a switched strain between 1 % and 500 %, and five cycles were carried out at fixed angular frequency (1 rad·s − 1).

5.2. In vivo experiments

Animals: All zebrafish lines were maintained in zebrafish facility under the standard conditions in Shanghai Tongren hospital at 28 °C, and the experiments were approved by the Animal Ethics Committee of Shanghai Tongren Hospital, China (A2023-123). Wild-type AB strain zebrafish and transgenic lines, including Tg (*mpeg1*: mCherry), Tg (*lyz*: EGFP) and Tg (*mnx1*: GFP), were used in the present study. 0.003 % 1-phenyl-2-thiourea (PTU, P7629, Sigma, USA) was added to the embryo medium to reduce pigmentation post fertilization at 12hpf (hour post fertilization).

Biocompatibility test: Zebrafish embryos were randomized to each group with 50 embryos. The hydrogel was put in the transwell upper chamber and co-cultured with 20 μl, 100 μl and 500 μl hydrogel for testing the biocompatibility of TPHD and TPHD@Tc (0.032 mg/ml) with gradient concentrations. The morphologies of larvae were observed at 48hpf and 72hpf, respectively. The survival rate was calculated at 48hpf, and the heart and hatching rate were counted at 72hpf.

Spinal cord injury model of zebrafish: At 3dpf (day post fertilization), zebrafish larvae were anesthetized in embryo medium containing 0.02 % tricaine (E10521, Sigma). Zebrafish larvae were transferred to a 35 mm petri dish with agarose (A620014, BBI) coated and placed in a lateral position. The 30 1/2 G syringe needle was used to achieve a spinal cord lesion between 17th and 20th somite. The SCI zebrafish larvae were randomized to Normal, SCI, TPHD, and TPHD@Tc. The TPHD and TPHD@Tc groups were treated with 100 μl hydrogel and hydrogel containing 0.32 mg/ml Tc from 3 dpf to 5dpf, respectively. Zebrafish were anesthetized and mounted in 1 % low melting agarose (A104063, Aladdin) with the confocal chamber (BS-20-GJM, Biosharp, China) and imaged with Confocal microscopes (Lecia, SP8, Germany).

Measurement of spinal cord bridging: Axonal bridging of zebrafish was detected using confocal microscopes (Lecia, SP8, Germany) at the 6hpi (hour post injury), 24hpi and 48hpi. mnx1-GFP labeled axon between the two spinal cord stumps was defines as “new axonal bridges”. The area fluorescence of axonal bridges was measured by ImageJ.

Swimming capability assay: The SCI surgery was performed at 5dpf on zebrafish larvae, then the SCI zebrafish larvae were divided into Normal, SCI, TPHD, and TPHD@Tc. The zebrafish were transferred to the 48-well culture plate. After therapy for 24 h and 48 h, the swimming performance were record by a high-speed camera. Trajectories of zebrafish movement were recorded by Zebrafish Behavior Track Tracking System (Noldus, Netherlands).

Macrophages and neutrophils imaging of zebrafish larvae: Tg (*mpeg1: mCherry*) and Tg (*lyz: EGFP*) zebrafish larvae were anesthetized and performed SCI surgery at 3dpf. Then the zebrafish larvae were incubated with TPHD and TPHD@Tc for 6 h, 24 h and 48 h and the zebrafish larvae were anesthetized and mounted in 1.5 % low melting agarose (A104063, Aladdin) with confocal chamber (BS-20-GJM, Biosharp). Macrophages and neutrophils images of zebrafish SCI lesion site were obtained by confocal microscope (Lecia, SP8, Germany).

RNA sequencing (RNA-seq): Zebrafish larvae were performed SCI surgery at 3 dpf, then the zebrafish were incubated with TPHD and TPHD@Tc for 24 h. The trunk of zebrafish including the SCI injury site was collected, and total mRNA was extracted using the RNA-easy Isolation Reagent (R701-01, Vazyme). RNA purity and quantification were determined using the NanoDrop 2000 spectrophotometer (Thermo Scientific). Then the VAHTS Universal V6 RNA-seq Library Prep Kit was used for constructed the libraries according to the manufacturer’s instructions. The transcriptome sequencing was performed by OE Biotech Co., Ltd. (Shanghai, China). DESeq2 was used to analysis of the differential expression. Thethreshold for significantly differentially expressed genes was q value < 0.05 and $|\log_2 FC| > 0.58$. GO and KEGG enrichment analysis of differentially expressed genes were performed to screen the significant enriched term using R (v 3.2.0), respectively. The Autophagy Database (https://www.autophagy.lu/index.html) and the genes published involved in autophagy process based on NCBI Pubmed (https://pubmed.ncbi.nlm.nih.gov) were collected as the autophagy-related gene set for Venn analysis. Venn analysis was then performed according to the different expression genes analyzed by RNA-Seq and autophagy related genes.

5.3. In vitro experiments

Cell line and treatment: Mouse microglia cell line (BV2) was purchased from Shanghai Zhong Qiao Xin Zhou Biotechnology co.,Ltd (ZQ0397). BV2 was cultured with DMEM (11965–092, Gibco) containing 10 % fetal bovine serum (FBS, 10099141C, Gibco) and 1 % penicillin/streptomycin (PS, G4003-100ML, Servicebio). Cells were stimulated by 100 ng/ml LPS (L2880, Sigma) for 1 or 4 days to activate M1 type microglia for further experiments.

Viability of BV2 cultured with hydrogel: BV2 at the density of 1×10^5 cells/well were seeded onto the *trans*-well plates (Corning, CLS3460), then the cells were co-cultured with TPHD, TPHD@TcL (0.016 mg/ml), TPHD@Tc (0.032 mg/ml), and TPHD@TcH (0.064 mg/

ml) for 12 h, 24 h and 96 h. Subsequently, DMEM containing 10 % Alamar Blue (DAL1100, invitrogen, Thermo Fisher Scientific) was replaced with BV2 cultured medium (DMEM containing 10 % FBS and 1 % PS) and incubated for 4 h. Then the absorbance of the supernatant was measured at 570 nm and 610 nm by Microplate Reader (Multiskan GO, Thermo Fisher Scientific, USA).

Reactive oxygen species (ROS) assay: BV2 cells were seeded into transwell plates with a density of 1×10^5 cells per well. LPS-induced BV2 cells were co-cultured with TPHD, TPHD@TcL, TPHD@Tc and TPHD@TcH for 1 day and 4 days. The ROS were detected by the Reactive Oxygen Species Assay Kit (S0033S, Beyotime) according to the manufacturer's instructions. Briefly, 10 μM 2,7-dichlorofluorescin diacetate (DCFH-DA) probe was incubated with the cells at 37 °C for 30 min in the dark cell incubator. Then, the cells were immediately observed under confocal microscope (Lecia, SP8, Germany). The relative fluorescence intensity of DCFH-DA positive fluorescence was quantified by DAPI using ImageJ software.

Microglia phenotype detection: BV2 cells were seeded into transwell plates with the density of 1×10^5 cells per well. LPS-induced BV2 cells were seed on the cell crawling slides with TPHD, TPHD@TcL, TPHD@Tc, TPHD@TcH in the upper chamber for 4 days. At the designed time points, the cells were rinsed with PBS and fixed with 4 % paraformaldehyde (PFA, P0099, Beyotime) for overnight. Samples were blocked with 1 % BSA (ST023, Beyotime) for 30 min and incubated with anti-iNOS (1:200, 22226–1-AP, Rabbit, Proteintech), anti-Arg1 (1:200, NB100-59740, Goat, NOVUS and anti-Iba1 antibody (1:100, sc-32725, mouse, Santa Curz) overnight at 4 °C. Then, the samples were rinsed with PBST for 3 times and followed incubated with CoraLite594-conjugated Goat Anti-Rabbit IgG(H + L) (1:250, SA00013-4, Goat, Proteintech), Cy3 conjugated Donkey Anti-Goat IgG (H + L) (1:300, GB21404, Donkey, Servicebio) and CoraLite488-conjugated Goat Anti-Mouse IgG(H + L) (1:250, SA00013-1, Goat, Proteintech) secondary antibodies for 2 h. After that, the samples were rinsed with PBST for 3 times and stained nuclei with mounting solution (P0131, Beyotime) containing 4′,6-diamidino-2-phenylindole pihydrochloride (DAPI). The fluorescent images were captured by confocal microscopy (Lecia, SP8, Germany).

Immunofluorescent staining: LPS-induced or combined SSD-induced BV2 cells with the density of 1×10^5 cells/well were seeded onto the cell crawling slides in transwell plates and cocultured with TPHD, TPHD@TcL, TPHD@Tc, TPHD@TcH in the upper chamber for 4 days. Then the cells were rinsed with PBS and fixed with 4 % PFA for overnight. Cells were blocked with 1 % BSA for 30 min and incubated with anti-NLRP3 (1:200, Gb114320, Rabbit, Servicebio, China), and anti-ANT1(1:200, A15027, Rabbit, ABclonal, Wuhan, China) overnight at 4 °C. Then, the samples were rinsed with PBST for 3 times and followed incubated with CoraLite488-conjugated Goat Anti-Rabbit IgG(H + L) (1:250, SA00013-2, Goat, Proteintech, Chicago, USA) and CoraLite594-conjugated Goat Anti-Rabbit IgG(H + L) (1:250, SA00013-4, Goat, Proteintech) secondary antibodies for 2 h. After that, the samples were rinsed with PBST for 3 times and stained nuclei with mounting solution containing DAPI (P0131, Beyotime, Shanghai, China). The fluorescent images were captured by confocal microscopy (Lecia, SP8, Germany).

Autophagy detection: BV2 cells with the density of 1×10^5 cells/well were seeded onto transwell plate for 24 h and transfected with pCMV-mCherry-GFP-LC3B (D2816, Beyotime) for 12 h using Lipofectamine 3000 (L3000001, ThermoFisher). Then, the cells were treated with LPS and co-cultured with TPHD, TPHD@TcL, TPHD@Tc, TPHD@TcH for 4 days. The mCheery-GFP-LC3B fusion protein was detected with the Confocal microscope (Lecia, SP8, Germany).

Mitophagy detection: BV2 cells with the density of 1×10^5 cells/well were seeded onto transwell plates and cultured for 24 h. Then, BV2 cells were transfected with pOPTN-EGFP (#27052, Addgene) using Lipofectamine 3000 (L3000001, ThermoFisher) and incubated for 12 h. Then the cells were treatment with LPS, TPHD, TPHD@TcL, TPHD@Tc, TPHD@TcH for 4 days. After that, the cells were performed IF staining with anti-Tomm20 (1:250, Rabbit, ab186735, Abcam) followed by CoraLite594-conjugated Goat Anti-Rabbit IgG(H + L) (1:250, SA00013-4, Goat, Proteintech). For mitophagy analysis, the damaged spherical mitochondria wrapped or chimeric by OPTN rings were captured by confocal microscopy (Lecia, SP8, Germany).

Western blotting analysis: BV2 cells with the density of 1×10^5 cells/well were seeded onto transwell plate (Corning, CLS3460). BV2 cells were induced by LPS and treated with TPHD, TPHD@TcL, TPHD@Tc, TPHD@TcH for 4 days. Then the BV2 cells were collected and lysed with Radio Immunoprecipitation Assay solution (RIPA, P0013K, Beyotime biotechnology) containing 1 mM Phenylmethanesulfonyl fluoride (PMSF, ST505, Beyotime biotechnology). The supernatant was collected by centrifugation at 12000 rpm for 15 min. BCA kit (23225, Thermo Fisher Scientific) was used for protein concentration measurement. 10μg extracted proteins were separated by 4 %-12 % SmartPAGE Precast Protein Gel (SLE001, Smart-Lifesciences) and then the protein was transferred to polyvinylidene difluoride (PVDF) membranes (IPVH00010, Millipore). Subsequently, the membranes were blocked with 1 % BSA for 2 h. Then the membranes were incubated with primary antibodies overnight at 4 °C, and then incubated with secondary antibody for 1 h. Finally, the membranes were imaged with Tanon 6200 (Tanno, Shanghai). The primary antibodies of NLRP3 (1:1000, Rabbit, ab263899, Abcam), ANT1 (1:1000, Rabbit, NBP2-92642, NOVUS), and the secondary antibodies of HRP-conjugated Affinipure Goat Anti-Rabbit IgG (H + L) (1:5000, SA00001-2, Proteintech) were used.

Quantitative RT-PCR: BV2 cells with the density of 1×10^5 cells/well were seeded onto transwell plate (Corning, CLS3460). BV2 cells were induced by LPS and treated with TPHD, TPHD@TcL, TPHD@Tc, TPHD@TcH for 4 days. Total RNA was extracted from BV2 cells with RNA-easy Isolation Reagent (R701-01, Vazyme) according to manufacturer's protocol. NanoDrop 2000 was used for evaluated the concentrations of RNA samples. PrimeScript™ RT Master Mix (Perfect Real Time) (RR036A, Takara) was utilized to reverse transcribed of mRNA to cDNA according to the instruction. The qPCR was performed as we previously reported[39]. Briefly, qPCR was performed with NLRP3, ANT1 and GAPDH-primers on ABI StepOne plus with PowerUP SYBR Green Master Mix (A25742, ThermoFisher). The primer sequences were listed below. The primer sequences for qPCR were listed in Table 1.

OPTN inhibition and inflammation detection: To further verify the effect of ANT1/OPTN axis on inflammation, the inhibitor, Saikosaponin D (SSD, HY-N0250, MCE), was used to suppress the OPTN protein expression level [40]. 5 μM SSD was used to repress OPTN in LPS-induced BV2 cells. BV2 cells with the density of 1×10^5 cells/well were seeded onto the lower chamber and TPHD, TPHD@TcL, TPHD@Tc, TPHD@TcH were put in upper chamber of transwell plate. Then the BV2 cells were stimulated with LPS and 5 μM SSD. After cultured for 4 days, WB, PCR and immunofluorescent staining were applied to detected the inflammation response after inhibiting OPTN. The detailed experimental processed please refer to the preceding part of the text.

Statistical analysis: GraphPad Prism (Version 9.0, GraphPad Software, USA) was used for data analysis. The unpaired Student's *t*-test was used to compare the two groups. For multiple groups comparison, one-way ANOVA followed by Bonferroni multiple comparisons test were used.

Table 1
Primer sequences for qPCR.

Gene name	Forward primer	Reverse primer
NLRP3	GACTGCGAGAGATTCTACAGC	CCTCCTCTTCCAGCAAATAGT
ANT1	GGTCTCTACCAGGGTTTCAGT	CTTGGCAGTGTCATAGACTCC
β-Actin	CACTGTCGAGTCGCGTCC	TCATCCATGGCGAACTGGTG
GAPDH	CCGCATCTTTGTGCAGTG	CGATACGGCCAAATCCGTTC

CRediT authorship contribution statement

Xiaohua Dong: Writing – original draft, Visualization, Software, Methodology, Formal analysis, Data curation. **Jing Zhao:** Writing – original draft, Visualization, Software, Methodology, Formal analysis, Data curation. **Dongya Jiang:** Data curation. **Ziyi Lu:** Data curation. **Xingdan Liu:** Data curation. **Kaijia Tan:** Data curation. **Kelvin W.K. Yeung:** Writing – review & editing. **Xuanyong Liu:** Writing – review & editing. **Liping Ouyang:** Writing – review & editing, Project administration, Funding acquisition, Conceptualization.

Declaration of competing interest

The authors declare that they have no known competing financial interests or personal relationships that could have appeared to influence the work reported in this paper.

Data availability

Data will be made available on request.

Acknowledgments

Funding: Financial support from the Laboratory Open Fund of Key Technology and Materials in Minimally Invasive Spine Surgery (2024JZWC-ZDB03), the National Natural Science Foundation of China (U21A20100), Research Fund of Shanghai Tongren Hospital, Shanghai Jiaotong University School of Medicine (2023DHYGJC-YBA01), the Fundamental Research Funds for The Central Universities (YG2023ZD29), the Talent project of Shanghai Tongren Hospital (TRKYRC-xx02, TR2023rc01), the Fundamental Research Funds for the Central Universities (2232023A-10) and the National Natural Science Foundation of China (82101621) are acknowledged.

Author contributions: Xiaohua Dong and Jing Zhao contributed equally to this work. Xiaohua Dong and Jing Zhao: Data curation, Methodology, Formal analysis, Visualization, Data collection, Software, Writing – original draft. Dongya Jiang: Data collection, Date curation. Ziyi Lu, Xingdan Liu and Kaijia Tan: Data Curation. Kelvin W. K. Yeung: Writing-Review & editing. Xuanyong Liu: Writing-Review & editing. Liping Ouyang: Conceptualization, Writing-Review & editing, Funding acquisition, Project administration.

Ethical approval: The experimental protocol concerning animals used in this work was approved by the Shanghai Tongren Hospital Ethics Committee (A2023-123) and (A2023-124).

Appendix A. Supplementary data

Supplementary data to this article can be found online at https://doi.org/10.1016/j.cej.2024.152263.

References

[1] Lagu Tara, Schroth Samantha L., Haywood Carol, Heinemann Allen, Kessler Allison, Morse Leslie, Khan Sadiya S., Kershaw Kiarri N., Nash Mark S. Diagnosis and Management of Cardiovascular Risk in Individuals With Spinal Cord Injury: A Narrative Review. Circulation 2023, 148: 268-277.

[2] M.A. Tarnopolsky, B.M. Flint, Potential for creatine and other therapies targeting cellular energy dysfunction in neurological disorders, Ann. Neurol. 49 (2001) 561–574.

[3] Hu Xiaoming, Leak Rehana K., Shi Yejie, Suenaga Jun, Gao Yanqin, Zheng Ping, Chen Jun. Microglial and macrophage polarization—new prospects for brain repair. Nature Reviews Neurology 2014, 11: 56-64.

[4] S. Kaoru, C.K. Glass, Microglial cell origin and phenotypes in health and disease, Nat. Rev. Immunol. 11 (2011) 775–787.

[5] Y. Jiang, P. Fu, Y. Liu, C. Wang, P. Zhao, X. Chu, X. Jiang, W. Yang, Y. Wu, Y. Wang, G. Xu, J. Hu, W. Bu, Near-infrared light-triggered NO release for spinal cord injury repair, Sci. Adv. 6 (2020).

[6] Liu Dongfei, Chen Jian, Jiang Tao, Li Wei, Huang Yao, Lu Xiyi, Liu Zehua, Zhang Weixia, Zhou Zheng, Ding Qirui, Santos Hélder A., Yin Guoyong, Fan Jin. Biodegradable Spheres Protect Traumatically Injured Spinal Cord by Alleviating the Glutamate-Induced Excitotoxicity. *Advanced Materials* 2018, 30: 1706032.

[7] F. Feng, S. Xiyong, Tu. Tan Zan, X.L. Yujie, X. Pengfei, Ma. Yahao, S. Xiumin, Ma. Junwu, R. Limin, H.e. Liumin, Cooperative assembly of a designer peptide and silk fibroin into hybrid nanofiber gels for neural regeneration after spinal cord injury, Sci. Adv. 9 (2023).

[8] M. Markus, G.F. King, D.J. Adams, P.F. Alewood, Trends in peptide drug discovery, Nat. Rev. Drug Discov. 20 (2021) 309–325.

[9] Y. Xin-Wang, W. Ying, S. Jun, L.i. Shan-Shan, Z. Bai-Yu, Y. Sai-Ge, W. Zi-Qi, L. Nai-Xin, L.i. Yi-Lin, W. Si-Yu, S. Yu-Heng, Z. Jian, W. Li-Juan, Z. Yue, A new peptide, VD11, promotes structural and functional recovery after spinal cord injury, Neural Regen. Res. 18 (2023).

[10] Wu. Wutian, L.v. Shi-Qin, ISP and PAP4 peptides promote motor functional recovery after peripheral nerve injury, Neural Regen. Res. 16 (2021).

[11] Yu. Fei, Xu. Yuan Yusong, N.S. Hailin, H. Na, Z. Yajun, Y. Xiaofeng, K. Yuhui, J. Baoguo, Neutrophil peptide-1 promotes the repair of sciatic nerve injury through the expression of proteins related to nerve regeneration, Nutr. Neurosci. 25 (2020) 631–641.

[12] Cao Zhongwei, Lis Raphael, Ginsberg Michael, Chavez Deebly, Shido Koji, Rabbany Sina Y., Fong Guo-Hua, Sakmar Thomas P., Rafii Shahin, Ding Bi-Sen. Targeting of the pulmonary capillary vascular niche promotes lung alveolar repair and ameliorates fibrosis. Nat. Med. 2016, 22: 154-162.

[13] Z. Sheng, Y. Jingwen, G.e. Zhuowang, X. Yi, Z. Min, J. Li, Activation of CXCR7 alleviates cardiac insufficiency after myocardial infarction by promoting angiogenesis and reducing apoptosis, Biomed. Pharmacother. 127 (2020) 110168.

[14] Wang Yanling, Li Guangnan, Stanco Amelia, Long Jason E., Crawford Dianna, Potter Gregory B., Pleasure Samuel J., Behrens Timothy, Rubenstein John L. R. CXCR4 and CXCR7 Have Distinct Functions in Regulating Interneuron Migration. Neuron 2011, 69: 61-76.

[15] Hilla Alexander M., Baehr Annemarie, Leibinger Marco, Andreadaki Anastasia, Fischer Dietmar. CXCR4/CXCL12-mediated entrapment of axons at the injury site compromises optic nerve regeneration. Proceedings of the National Academy of Sciences 2021, 118.

[16] Rao Jia-Sheng, Zhao Can, Zhang Aifeng, Duan Hongmei, Hao Peng, Wei Rui-Han, Shang Junkui, Zhao Wen, Liu Zuxiang, Yu Juehua, Fan Kevin S., Tian Zhaolong, He Qihua, Song Wei, Yang Zhaoyang, Sun Yi Eve, Li Xiaoguang. NT3-chitosan enables de novo regeneration and functional recovery in monkeys after spinal cord injury. Proceedings of the National Academy of Sciences 2018, 115.

[17] Yang Zhaoyang, Zhang Aifeng, Duan Hongmei, Zhang Sa, Hao Peng, Ye Keqiang, Sun Yi E., Li Xiaoguang. NT3-chitosan elicits robust endogenous neurogenesis to enable functional recovery after spinal cord injury. Proceedings of the National Academy of Sciences 2015, 112: 13354-13359.

[18] Li Liming, Xiao Bing, Mu Jiafu, Zhang Yu, Zhang Chenyang, Cao Hongcui, Chen Rongjun, Patra Hirak Kumar, Yang Bo, Feng Shiqing, Tabata Yasuhiko, Slater Nigel K. H., Tang Jianbin, Shen Youqing, Gao Jianqing. A MnO2 Nanoparticle-Dotted Hydrogel Promotes Spinal Cord Repair via Regulating Reactive Oxygen Species Microenvironment and Synergizing with Mesenchymal Stem Cells. ACS Nano 2019, 13: 14283-14293.

[19] Xu. Liu Weiyuan, Z.S. Bai, H. Shuyu, Q. Rui, L. Wenbin, J.i. Chunnan, C. Bing, X. Zhifeng, Y. Man, Y. Yanyun, D. Jianwu, Z. Yannan, Spinal cord tissue engineering via covalent interaction between biomaterials and cells, Sci. Adv. 9 (2023).

[20] Shan Bai-Hui, Wu Fu-Gen. Hydrogel-Based Growth Factor Delivery Platforms: Strategies and Recent Advances. Advanced Materials 2023.

[21] Yu. Wang Xiaocheng, Y.C. Yunru, S. Luoran, Z. Yuanjin, S. Xian, Dynamically Responsive Scaffolds from Microfluidic 3D Printing for Skin Flap Regeneration, Adv. Sci. 9 (2022).

[22] Siebert Leonard, Luna-Cerón Eder, García-Rivera Luis Enrique, Oh Junsung, Jang JunHwee, Rosas-Gómez Diego A., Pérez-Gómez Mitzi D., Maschkowitz Gregor, Fickenscher Helmut, Oceguera-Cuevas Daniela, Holguín-León Carmen G., Byambaa Batzaya, Hussain Mohammad A., Enciso-Martínez Eduardo, Cho Minsung, Lee Yuhan, Sobahi Nebras, Hasan Anwarul, Orgill Dennis P., Mishra Yogendra Kumar, Adelung Rainer, Lee Eunjung, Shin Su Ryon. Light-Controlled Growth Factors Release on Tetrapodal ZnO-Incorporated 3D-Printed Hydrogels for Developing Smart Wound Scaffold. Advanced Functional Materials 2021, 31.

[23] H. Wei-Chen, L. Chun-Chang, C. Tzai-Wen, C. San-Yuan, 3D Gradient and Linearly Aligned Magnetic Microcapsules in Nerve Guidance Conduits with Remotely Spatiotemporally Controlled Release to Enhance Peripheral Nerve Repair, ACS Appl. Mater. Interfaces 14 (2022) 46188–46200.

[24] Han Qi, Ordaz Josue D., Liu Nai-Kui, Richardson Zoe, Wu Wei, Xia Yongzhi, Qu Wenrui, Wang Ying, Dai Heqiao, Zhang Yi Ping, Shields Christopher B., Smith George M., Xu Xiao-Ming. Descending motor circuitry required for NT-3 mediated locomotor recovery after spinal cord injury in mice. Nat Commun 2019, 10.

[25] Y. Wang, E.R. Zoneff, J.W. Thomas, N. Hong, L.L. Tan, D.J. McGillivray, A. W. Perriman, K.C.L. Law, L.H. Thompson, N. Moriarty, C.L. Parish, R.J. Williams, C.J. Jackson, D.R. Nisbet, Hydrogel oxygen reservoirs increase functional integration of neural stem cell grafts by meeting metabolic demands, Nat Commun 14 (2023).

[26] S. Joachim, C.J. Woolf, The neuropathic pain triad: neurons, immune cells and glia, Nat Neurosci 10 (2007) 1361–1368.

[27] V. Deretic, Autophagy in inflammation, infection, and immunometabolism, Immunity 54 (2021) 437–453.

[28] A. Hoshino, W.J. Wang, S. Wada, C. McDermott-Roe, C.S. Evans, B. Gosis, M. P. Morley, K.S. Rathi, J. Li, K. Li, S. Yang, M.J. McManus, C. Bowman, P. Potluri, M. Levin, S. Damrauer, D.C. Wallace, E.L.F. Holzbaur, Z. Arany, The ADP/ATP

translocase drives mitophagy independent of nucleotide exchange, Nature 575 (2019) 375–379.
[29] P. Konstantinos, L. Eirini, T. Nektarios, Mechanisms of mitophagy in cellular homeostasis, physiology and pathology, Nat Cell Biol 20 (2018) 1013–1022.
[30] L. Zhou, L. Fan, X. Yi, Z. Zhou, C. Liu, R. Fu, C. Dai, Z. Wang, X. Chen, P. Yu, D. Chen, G. Tan, Q. Wang, C. Ning, Soft Conducting Polymer Hydrogels Cross-Linked and Doped by Tannic Acid for Spinal Cord Injury Repair, ACS Nano 12 (2018) 10957–10967.
[31] D. Samuel, K. Antje, Repertoire of microglial and macrophage responses after spinal cord injury, Nat. Rev. Neurosci. 12 (2011) 388–399.
[32] Z. Rongbin, A.S. Yazdi, M. Philippe, Tschopp Jürg. A role for mitochondria in NLRP3 inflammasome activation, Nature 469 (2010) 221–225.
[33] Harrington John S., Ryter Stefan W., Plataki Maria, Price David R., Choi Augustine M. K. Mitochondria in health, disease, and aging. Physiol. Rev. 2023, 103: 2349-2422.
[34] Harding Olivia, Holzer Elisabeth, Riley Julia F., Martens Sascha, Holzbaur Erika L. F. Damaged mitochondria recruit the effector NEMO to activate NF-κB signaling. Molecular Cell 2023, 83: 3188-3204.e3187.
[35] L. Qisheng, L.i. Shu, J. Na, J. Haijiao, S. Xinghua, Wu. Zhu Xuying, Z.M. Jingkui, Z. Zhen, S. Jianxiao, Gu. Zhou Wenyan, L.L. Renhua, N.i. Zhaohui, Inhibiting NLRP3 inflammasome attenuates apoptosis in contrast-induced acute kidney injury through the upregulation of HIF1A and BNIP3-mediated mitophagy, Autophagy 17 (2020) 2975–2990.
[36] W. Hongyun, Y.e. Junrui, P. Ye, Ma. Wenyu, C. Haodong, S. Hongshuo, F. Zhongping, H.e. Wenbin, L.i. Gang, C.u. Shifeng, Z. Zhao, C. Naihong, CKLF induces microglial activation via triggering defective mitophagy and mitochondrial dysfunction, Autophagy (2023) 1–24.
[37] M.J. Bround, D.M. Bers, J.D. Molkentin, A 20/20 view of ANT function in mitochondrial biology and necrotic cell death, J. Mol. Cell Cardiol. 144 (2020) A3–A13.
[38] Z. Sheng, Y. Jingwen, G.e. Zhuowang, X. Yi, Z. Min, J. Li, Activation of CXCR7 alleviates cardiac insufficiency after myocardial infarction by promoting angiogenesis and reducing apoptosis, Biomed. Pharmacother. 127 (2020).
[39] X. Dong, D. Jiang, L. Wang, J. Zhao, L. Yu, Y. Huang, X. Wu, Y. Zhu, Y. Zhao, Q. Zhao, G. Zhang, X. Li, VPS28 regulates brain vasculature by controlling neuronal VEGF trafficking through extracellular vesicle secretion, iScience 25 (2022) 104042.
[40] Wang Jiajia, Wang Jiaying, Hong Wenxiang, Zhang Lulu, Song Liqian, Shi Qi, Shao Yanfei, Hao Guifeng, Fang Chunyan, Qiu Yueping, Yang Lijun, Yang Zhaoxu, Wang Jincheng, Cao Ji, Yang Bo, He Qiaojun, Weng Qinjie. Optineurin modulates the maturation of dendritic cells to regulate autoimmunity through JAK2-STAT3 signaling. Nat Commun 2021, 12.